



City Research Online

City, University of London Institutional Repository

Citation: Wei, Z., Yang, B., You, Q., Tsavdaridis, K. D. & Jia, S. (2025). Study on multi-parameter optimization of seismic isolation bearings for continuous girder bridges considering interactions among key parameters. *Scientific Reports*, 15(1), 18448. doi: 10.1038/s41598-025-02155-z

This is the accepted version of the paper.

This version of the publication may differ from the final published version.

Permanent repository link: <https://openaccess.city.ac.uk/id/eprint/35311/>

Link to published version: <https://doi.org/10.1038/s41598-025-02155-z>

Copyright: City Research Online aims to make research outputs of City, University of London available to a wider audience. Copyright and Moral Rights remain with the author(s) and/or copyright holders. URLs from City Research Online may be freely distributed and linked to.

Reuse: Copies of full items can be used for personal research or study, educational, or not-for-profit purposes without prior permission or charge. Provided that the authors, title and full bibliographic details are credited, a hyperlink and/or URL is given for the original metadata page and the content is not changed in any way.

City Research Online:

<http://openaccess.city.ac.uk/>

publications@city.ac.uk

Study on multi-parameter optimization of seismic isolation bearings for continuous girder bridges considering interactions among key parameters

Zhaolan Wei^{1,2,*}, Bowen Yang¹, Qixuan You¹, Konstantinos Daniel Tsavdaridis², Shaomin Jia¹

¹ School of Civil Engineering, Sichuan Agricultural University, Chengdu 611830, China

² Department of Engineering, School of Science & Technology, City, University of London, Northampton Square, London, EC1V 0HB London, UK.

* Correspondence: wzhl@sicau.edu.cn; Tel.: +86 13880971586

Abstract

Traditional isolation design for continuous girder bridges often focuses on single-parameter tuning, overlooking the complex interactions among yield strength, pre-yield stiffness, and post-yield stiffness. This paper proposes a multi-parameter optimization method to systematically investigate the nonlinear influence of each parameter on the seismic performance of bridges. First, using a conventional particle swarm optimization (PSO) algorithm, the individual and combined effects of each parameter on key response indicators are identified. On this basis, an adaptive particle swarm optimization (APSO) algorithm with dynamic inertia weights and learning factors is introduced to broaden the search space, expedite convergence, and reduce the likelihood of becoming trapped in local optima. Numerical studies indicate that, compared with the standard PSO method, APSO can reduce the total number of iterations by up to 40% while maintaining solution accuracy. The underlying mechanism is that APSO preserves particle diversity and dynamically adjusts the balance between global and local searches, thereby rapidly identifying the optimal bearing configuration. Compared with single-parameter or orthogonal design methods, the APSO-based multi-parameter optimization strategy significantly enhances structural ductility, as reflected by notable reductions in pier-top displacement and pier-bottom shear force. These findings underscore the robustness and efficiency of APSO in designing isolation bearings for high-dimensional problem spaces.

1 Introduction

Major earthquakes, such as the 1995 Hanshin-Awaji Earthquake in Japan and the 2008 Wenchuan Earthquake in China, have repeatedly underscored the significant vulnerability of bridges during large-scale seismic events¹. For bridge structures located in areas of intense seismic activity, the failure of any component can lead to immense economic losses and severely disrupt post-disaster rescue and reconstruction efforts. In response, seismic isolation technology has gained increasing prominence in bridge engineering, as it effectively decouples the superstructure from seismic motions and thus mitigates structural damage. Among these technologies, isolation bearings play a pivotal role in dissipating seismic energy; their performance is crucial for ensuring bridge safety and functionality under strong earthquakes². In areas prone to high-intensity seismic activity, the careful selection of optimal bearing parameters can markedly improve the reliability and serviceability of continuous girder bridges, thereby securing lifeline transportation networks and facilitating rapid emergency response operations.

42 Although existing research has made notable strides in elucidating the nonlinear behavior of isolation
43 bearings, most work has focused on individual parameters, such as bearing yield strength or stiffness³.
44 Amiri et al.⁴ studied the seismic response of triple friction pendulum isolators under near-fault ground
45 motions, identifying through detailed sensitivity analysis the optimal bearing parameters that significantly
46 improve overall damping efficiency. Peng et al.⁵ proposed a reliability-based optimization framework for
47 adaptive sliding isolation systems, incorporating sensitivity analysis and magnetically sliding bearings to
48 enhance seismic performance. Zhong et al.⁶ developed a risk-driven sensitivity analysis and optimization
49 procedure based on Gaussian process surrogate models, effectively lowering seismic risk through refined
50 bearing parameter selection. Concurrently, Gur et al.⁷ focused on the stochastic optimization of shape
51 memory alloy rubber bearings, showing that such bearings can markedly boost isolation capacity under
52 random seismic scenarios. While these single-parameter approaches deepen our understanding of
53 isolation performance, they often prove inadequate for practical engineering applications, especially when
54 multiple parameters interact to shape the overall seismic response. For continuous girder bridges with
55 significant variations in pier heights, curvature effects, or other complex factors, relying solely on single-
56 parameter analyses risks overlooking critical coupling effects among bearing design variables.
57 Consequently, examining bearing design from a multi-parameter perspective not only aligns better with
58 real-world conditions but also offers a more comprehensive strategy for enhancing seismic safety.

59 To address the challenges inherent in multi-parameter design, researchers have increasingly adopted
60 computational intelligence methods—particularly PSO—to systematically identify optimal isolation
61 bearing parameters. For instance, Pang et al.⁸ formulated a risk-based design and optimization framework
62 for shape memory alloy-restrained sliding bearings in highway bridges subjected to near-fault seismic
63 loading, employing PSO to reduce seismic risk. Xia et al.⁹ introduced an improved PSO technique for
64 structural model updating in high-dimensional bridge systems, achieving higher accuracy and efficiency
65 using ambient vibration data. Tran-Ngoc et al.¹⁰ devised a hybrid model updating approach for multi-span
66 railway bridges, combining orthogonal diagonalization with an enhanced PSO algorithm to lower
67 computational complexity. Chen et al.¹¹ proposed an improved PSO-based analysis method for the
68 construction stages of suspension bridges, integrating the standard PSO with genetic algorithms to obtain
69 a more precise system configuration. Li et al.¹² adopted a novel PSO algorithm to develop an optimal
70 sensor placement strategy for long-span cable-stayed bridges, reducing costs while enhancing
71 measurement efficiency. Quaranta et al.¹³ employed differential evolution and PSO to identify key
72 parameters of isolation devices, confirming the feasibility of nontraditional techniques in isolator
73 characterization. Zhang et al.¹⁴ used PSO for simultaneous inversion of pre-stack seismic data, improving
74 elastic parameter models and bolstering both the precision and reliability of geophysical interpretations.
75 Similarly, recent machine learning approaches, such as Wei et al.¹⁵, employed extensive datasets to predict
76 seismic responses and fragility of high-speed railway bridges, showcasing strengths in predictive
77 efficiency but reliance on data availability. Additionally, Wei et al.¹⁶ introduced novel ductile piers with
78 improved deformation capabilities under seismic loads, potentially influencing the performance
79 requirements and optimization of isolation bearings. While various state-of-the-art optimization
80 algorithms such as Differential Evolution (DE), Genetic Algorithm (GA), Grey Wolf Optimizer (GWO),
81 and Ant Colony Optimization (ACO) have demonstrated success in structural optimization tasks, PSO
82 remains particularly well-suited for multi-parameter problems characterized by continuous search spaces,
83 nonlinearity, and complex constraint interactions. PSO has demonstrated consistent robustness and
84 efficiency specifically in engineering design optimization problems characterized by nonlinear, multi-
85 modal, and high-dimensional search spaces, typical of seismic isolation bearing optimization scenarios.
86 Compared to DE and GA, PSO typically requires fewer control parameters and exhibits faster
87 convergence in scenarios involving moderate noise or multimodal objective functions. Moreover, hybrid

88 PSO variants have been shown to outperform other algorithms in computational efficiency and robustness
89 when applied to civil engineering optimization tasks. Given the high-dimensional, nonlinear, and
90 computationally intensive nature of seismic isolation bearing design, PSO—especially in its enhanced,
91 adaptive forms—presents a compelling choice. The present study builds on this foundation by integrating
92 adaptive strategies into the PSO framework, specifically tailored to the physical constraints and seismic
93 demands of continuous girder bridges. Despite these advances, conventional PSO still faces challenges in
94 balancing convergence speed and robustness in design spaces with higher dimensionality and multiple
95 constraints. To tackle this issue, the present study introduces an improved particle swarm optimization
96 (APSO) that adaptively adjusts inertia weights and learning factors, thereby enhancing both optimization
97 efficiency and convergence speed. This improvement is especially advantageous for large-scale, nonlinear
98 isolation design problems, where computational efficiency is of paramount importance.

99 The primary novelty of this work lies in integrating multi-parameter isolation design with an enhanced
100 particle swarm algorithm specifically tailored for continuous girder bridges, thus forming a systematic
101 approach. By comprehensively considering critical nonlinear bearing characteristics under bidirectional
102 seismic excitation—namely yield strength, pre-yield stiffness, and post-yield stiffness—our study
103 transcends the limitations of single-parameter optimization. Moreover, we demonstrate that APSO not
104 only accelerates convergence but also improves the optimal isolation performance, making it more
105 effective than conventional PSO or other common optimization strategies under the complex conditions
106 typical of continuous girder bridges. In Section 2, we derive the particle swarm formulation for the multi-
107 parameter optimization of damping-isolation bearings, while in Section 3 we enhance the traditional PSO,
108 proposing an adaptive particle swarm algorithm. In Section 4, comparative experiments against
109 conventional optimization methods illustrate APSO’s superior performance in multi-parameter isolation
110 bearing design, offering theoretical insights and practical guidance for seismic bridge design.
111

112 **2 Optimization of damping-isolation bearings using particle** 113 **swarm optimization**

114 In the design of continuous girder bridges located in high-intensity seismic zones, isolation bearing
115 parameters play a pivotal role in determining the overall seismic performance of the structure.
116 Conventional optimization approaches often concentrate on a single parameter (e.g., yield strength or
117 stiffness) to reduce design complexity; however, such simplifications tend to overlook the interactions
118 among multiple bearing parameters under realistic seismic demands. Conversely, multi-parameter
119 optimization provides a holistic understanding of bearing responses under severe seismic excitations,
120 thereby markedly enhancing the resilience of critical transportation infrastructure¹⁷.

121 This section introduces the PSO algorithm and discusses its application in multi-parameter bearing
122 optimization. Compared with conventional methods, PSO offers strong global search capabilities and high
123 computational efficiency, making it particularly suitable for large-scale structural problems involving
124 nonlinear material behavior and multi-degree-of-freedom systems.

125 PSO is a classic intelligent optimization method. It typically uses a random strategy to initialize
126 multiple candidate solutions (particles) and then iteratively updates these solutions according to a
127 prescribed procedure until an optimal solution is found based on a certain fitness criterion. At each
128 iteration, particles are adjusted according to two “extreme” values within the swarm: the first is the
129 historical best solution found by the particle itself, denoted as $pBest$; the second is the historical best

130 solution found by the entire population, denoted as $gBest$ ^{18,19}.

131 The iterative process through which each particle seeks the optimal solution can be described
 132 mathematically by Equations (1) and (2)²⁰. In an n -dimensional target search space, the position and
 133 velocity of the d -th particle can be expressed as:

$$134 \quad X_i = \{x_{i1}, x_{i2}, \dots, x_{in}\}, i = 1, 2, \dots, n \quad (1)$$

$$135 \quad V_i = \{v_{i1}, v_{i2}, \dots, v_{in}\}, i = 1, 2, \dots, n \quad (2)$$

136 During iterative optimization, the $pBest$ and $gBest$ of the i -th particle at the current time, as well as
 137 their corresponding particle position vectors, can be represented by:

$$138 \quad pBest_i = \{pBest_{i1}, pBest_{i2}, \dots, pBest_{in}\}, i = 1, 2, \dots, n \quad (3)$$

$$139 \quad gBest_i = \{gBest_{i1}, gBest_{i2}, \dots, gBest_{in}\}, i = 1, 2, \dots, n \quad (4)$$

$$140 \quad \vec{P}_i = \{p_{i1}, p_{i2}, \dots, p_{in}\}, i = 1, 2, \dots, n \quad (5)$$

$$141 \quad \vec{G}_i = \{g_{i1}, g_{i2}, \dots, g_{in}\}, i = 1, 2, \dots, n \quad (6)$$

142 Throughout the iterative procedure, all particles in the swarm strictly search within a prescribed region,
 143 denoted by $\{R = D \mid D = (e_1, e_2, \dots, e_d), -X_d^{\max} \leq e_d \leq X_d^{\max}, d = 1, 2, \dots, D\}$. The maximum search range and
 144 maximum search speed for each particle are represented by $X^{\max} = \{x_1^{\max}, x_2^{\max}, \dots, x_i^{\max}\}$ and
 145 $V^{\max} = \{v_1^{\max}, v_2^{\max}, \dots, v_i^{\max}\}$, respectively. When $x_i > X_i^{\max}, v_i > V_i^{\max}$, set $x_i = X_i^{\max}, v_i = V_i^{\max}$; and when
 146 $x_i < -X_i^{\max}, v_i < -V_i^{\max}$, set $x_i = -X_i^{\max}, v_i = -V_i^{\max}$.

147 Particle positions are updated by $x_{id}^{t+1} = x_{id}^t + v_{id}^{t+1}$, following the iterative procedure outlined below:

148 (1) Initialize particle positions and velocities, setting initial solutions as each particle's individual
 149 best ($pBest_i$) positions and selecting the overall best as the global best ($gBest_i$).

150 (2) Calculate each particle's objective function (fitness).

151 (3) Update each $pBest_i$ if its current fitness is superior; similarly, update the $gBest_i$ if a new
 152 global optimum is identified.

153 (4) Update the d th-dimensional position and velocity for each particle i .

154 (5) Check whether the current solution satisfies the termination condition; if it does, output $gBest$
 155 and terminate. Otherwise, return to step (2) and continue iterating until the termination condition is met.
 156 In PSO, one of the most critical factors is the velocity update scheme, which plays a decisive role in both
 157 optimization performance and convergence speed. Typically, three commonly used formulas are adopted
 158 for velocity updating, as given in Equations (7), (9), and (11), with the corresponding position-update

formulas provided in Equations (8), (10), and (12).

$$v_{id}^{t+1} = v_{id}^t + c_1 r_1 (pBest_{id}^t - x_{id}^t) + c_2 r_2 (gBest_{id}^t - x_{id}^t) \quad (7)$$

$$x_{id}^{t+1} = x_{id}^t + v_{id}^{t+1} \quad (8)$$

where $i=1,2,\dots,n$ represents the individual particles, and n is the total number of particles; v_{id}^{t+1} is the d -dimensional velocity of the i -th particle at iteration $t+1$; v_{id}^t is the d -dimensional velocity of the i -th particle at iteration t ; c_1, c_2 are the learning factors for the $pBest$ and $gBest$, also known as acceleration constants, typically set to $c_1 = c_2 = 2$; r_1, r_2 are uniform random numbers within the range $(0, 1)$, which adjust the $pBest$ and $gBest$ to enhance the diversity of the swarm; x_{id}^{t+1} is the position of the particle after $t+1$ iterations; and x_{id}^t is the position of the particle after t iterations.

$$v_{id}^{t+1} = \theta v_{id}^t + c_1 r_1 (pBest_{id}^t - x_{id}^t) + c_2 r_2 (gBest_{id}^t - x_{id}^t) \quad (9)$$

$$x_{id}^{t+1} = x_{id}^t + v_{id}^{t+1} \quad (10)$$

where θ is the constraint factor, which is a constant coefficient in front of the velocity when the position is updated.

$$v_{id}^{t+1} = \omega v_{id}^t + c_1 r_1 (pBest_{id}^t - x_{id}^t) + c_2 r_2 (gBest_{id}^t - x_{id}^t) \quad (11)$$

$$x_{id}^{t+1} = x_{id}^t + v_{id}^{t+1} \quad (12)$$

where ω is referred to as the inertia factor, and its value is non-negative. In typical iterative optimization processes, ω is usually a dynamic value. It is generally more effective for optimization compared to a fixed value. The value of ω typically changes linearly, with the most commonly used strategy being the linear decreasing weight (LDW) strategy: $\omega^{(t)} = (\omega_{ini} - \omega_{end})(G_k - g) / G_k + \omega_{end}$, where G_k represents the maximum number of iterations, ω_{ini} is the initial inertia weight, and ω_{end} is the inertia weight at the maximum iteration. A typical choice for inertia weights is $\omega_{ini} = 0.9$ and $\omega_{end} = 0.4$. When the inertia weight is large, the global optimization ability is stronger, but the local optimization ability is weaker. When the inertia weight is small, the global optimization ability is weaker, but the local optimization ability is stronger.

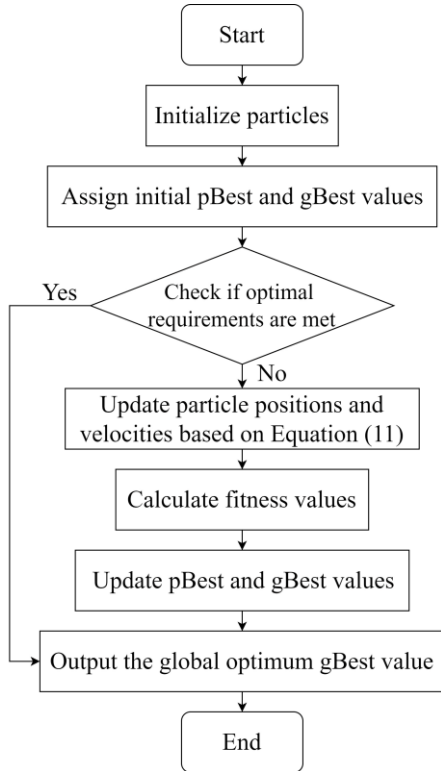
The polynomial formula consists of three terms:

(1) Inertia term: Retains particle velocity from the previous iteration, acting as a momentum to explore solution space.

(2) Self-cognitive term: Guides particles based on their own best-known position, reflecting individual experience and promoting local search efficiency.

(3) Social-cognitive term: Directs particles toward the global best-known solution, leveraging collective swarm experience to enhance convergence toward the global optimum.

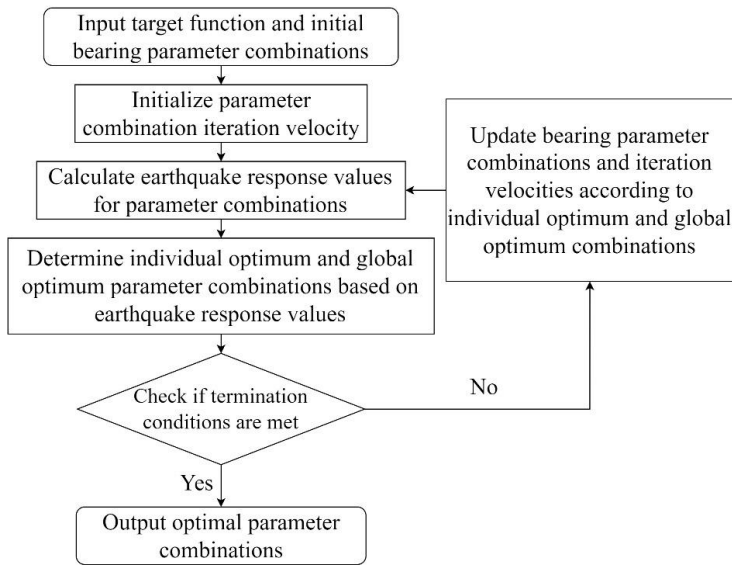
190 These components collectively influence both convergence speed and optimization performance, and
 191 standard velocity updating equations referenced in the manuscript are employed.
 192 Equations (7) and (9) are generally regarded as the standard forms of PSO.
 193 In summary, the basic principles of the particle swarm algorithm can be represented by the flowchart
 194 shown in Figure 1.



195
 196 **Figure 1.** Basic flow chart of PSO.

197 The PSO algorithm has opened new research and practical pathways in the field of seismic design for
 198 bridges. In the face of complex engineering challenges such as large-span bridges, traditional design
 199 methods often struggle to provide comprehensive and convenient solutions, especially when dealing with
 200 parameter optimization. Known for its flexibility and efficiency, the PSO algorithm is particularly suitable
 201 for solving multi-parameter optimization problems. By simulating the search behavior of particles within
 202 the parameter space, the PSO algorithm can explore a wide design space and comprehensively optimize
 203 the three nonlinear characteristic parameters of the bearings (yield strength, pre-yield stiffness, and post-
 204 yield stiffness). Considering the structural characteristics of seismic isolation continuous girder bridges,
 205 the application of PSO in parameter optimization focuses on reducing seismic impact and enhancing the
 206 adaptability of the structure, aiming to find the optimal combination of parameters that improve the
 207 performance of the bridge under seismic loading^{21,22}.

208 The flowchart for solving the multi-parameter optimization problem of damping isolation bearings using
 209 the PSO algorithm is shown in Figure 2.



210
211 **Figure 2.** PSO Algorithm for Solving Bearing Optimal Parameter Combinations Flowchart.

212 While the classic PSO algorithm demonstrates considerable strength in multi-parameter bearing
213 optimization, nonlinear and large-scale practical scenarios often require faster convergence and more
214 adaptive search strategies. To overcome these challenges, this study proposes an improved APSO
215 algorithm that dynamically adjusts key parameters to enhance both the optimization rate and iteration
216 speed. These enhancements broaden the scope of swarm intelligence in seismic isolation bearing design,
217 enabling safer and more cost-effective solutions in the complex engineering environments of earthquake-
218 prone regions.

219

220 3 Adaptive particle swarm optimization algorithm for seismic 221 isolation bearings in bridges

222 Although the multi-objective PSO algorithm has gained increasing popularity in the fields of structural
223 and seismic engineering due to its relatively simple algorithmic principles and fewer control parameters²³,
224 it still has certain limitations. Classic PSO often faces the issue of premature convergence when the search
225 space is large and complex. The particle swarm may converge to a local optimum early in the iteration
226 process, resulting in stagnation. If the distribution of particles in certain parameter dimensions (such as
227 yield strength, pre-yield stiffness, or post-yield stiffness) is too narrow or uneven, the swarm may become
228 stuck, hindering global optimization and slowing convergence.

229 These shortcomings highlight a core requirement in practical engineering applications: when optimizing
230 bearing parameters, an algorithm is needed that not only converges quickly but also possesses strong
231 global search capabilities. For bridges located in seismic zones, safety indices are crucial. Therefore, the
232 ability to effectively avoid local optima and find better solutions within a limited computational time
233 frame is particularly important.

234 To address this need, this paper proposes the Adaptive Particle Swarm Optimization (APSO) algorithm,
235 which systematically adapts the key parameters of the particle swarm (such as inertia factor, learning
236 factors, velocity and position update rules, and iteration termination conditions) to address these
237 challenges. During the optimization process, APSO dynamically adjusts various parameters to provide a
238 broader search space in the early stages (enhancing global exploration) and accelerate convergence in
239 later stages. These improvements make APSO more suitable for practical engineering projects, allowing
240 it to optimize faster and more robustly when dealing with multi-dimensional seismic isolation bearing

241 parameters.

242 The following sections will detail the specific improvements of APSO and explain how it effectively
243 addresses the shortcomings of classic PSO, achieving better results in multi-parameter seismic bearing
244 optimization.

245 (1) Improvement of Inertia Factor

246 It is generally believed that the inertia factor has the greatest impact on the iteration speed. The value of
247 the inertia factor plays a crucial role in both the global search ability and the search speed of the algorithm.
248 Since Shi introduced the linear inertia factor in 1998, many scholars have proposed different methods for
249 assigning inertia factor values based on different problems. However, most of these methods perform well
250 only for specific problems and lack strong general applicability²⁴.

251 In this paper, a new adaptive inertia factor is introduced for the multi-parameter optimization of damping
252 isolation bearings. This adaptive inertia factor allows the iteration process to decrease slowly in the early
253 stages to expand the search range of particles, decrease more rapidly in the middle stages to improve
254 iteration speed and efficiency, and decrease slowly in the later stages to allow particles to fine-tune their
255 search near the optimal solution, enhancing accuracy. The use of the exponential term ensures that the
256 adjustment of the inertia factor is smooth and continuous, facilitating better balance between exploration
257 and exploitation throughout the optimization process. The value assignment method for this adaptive
258 inertia factor is given by Equation (13).

$$259 \quad \omega_d = \omega_{end} + (\omega_{ini} - \omega_{end}) \times e^{\left[k \cdot \sigma_{(t)}^\theta \right]} \quad (13)$$

260 where $\sigma_{(t)}$ is the fitness value dispersion coefficient during the iteration process; k and θ are
261 experimental constants determined by the initial fitness value. Typically, the optimal values are selected
262 by conducting multiple simulations and observing the resulting search efficiency and convergence
263 behavior of the optimization algorithm.

264 The fitness value dispersion coefficient is the ratio of the standard deviation to the mean value of the data
265 set, expressed as a percentage. The common calculation formula for this is shown in Equation (14).

$$266 \quad \sigma_{(t)} = \frac{C}{\bar{X}} \times 100\% \quad (14)$$

267 where C represents the data standard deviation; \bar{X} represents the data mean value.

268 (2) Improvement of Learning Factors

269 The inertia factor primarily determines the speed of the iterating particles, while the learning factor
270 governs the learning of the individual best position and the global best position. In the standard PSO
271 algorithm, the learning factor is usually fixed as a constant. Such a constant learning factor lacks
272 variability and flexibility, thus having little positive impact on the algorithm. Therefore, to enhance the
273 learning factor's positive effect, the general constant learning factor is replaced with a linear learning
274 factor: In the early stages, to expand the search range, the emphasis should be on the influence of the
275 individual best position; in the later stages, to more quickly and accurately find the optimal solution, the
276 focus should shift to the influence of the global best position. Unlike the inertia factor, exponential decay
277 usually reduces the learning factor quickly in the early stages of the optimization process, which may
278 cause particles to be too concentrated near the global optimal solution too early, reducing the diversity of
279 exploration. This may cause the algorithm to fall into a local optimal solution without enough
280 opportunities to explore the entire search space. The value assignment method for this learning factor is
281 shown in Equation (15).

$$\begin{cases} c_1^t = c_1^{ini} + \frac{(G_k - g)(c_1^{ini} - c_1^{end})}{G_k} \\ c_2^t = c_2^{ini} + \frac{(G_k - g)(c_2^{ini} - c_2^{end})}{G_k} \end{cases} \quad (15)$$

where c_1^t, c_2^t represent the values of the learning factors during the iteration process; c_1^{ini}, c_1^{end} are the starting and final values of the c_1 learning factor; c_2^{ini}, c_2^{end} are the starting and final values of the c_2 learning factor; G_k represents the maximum number of iterations; g represents the individual particles.

(3) Improvement of Position Update Method

The direction and position of a particle during iteration are primarily controlled by the individual best and global best positions. This often leads to the particles becoming trapped in local optima and overlooking better positions within the particle's neighborhood. To reduce this occurrence, a certain range of neighborhood intervals, $[pBest_i^t(1-r(0,1)), pBest_i^t(1+r(0,1))]$ and $[gBest_i^t(1-r(0,1)), gBest_i^t(1+r(0,1))]$, is added around the individual best and global best positions, allowing the particles to perform a neighborhood random search within these specific regions.

(4) Improvement of Iteration Termination Conditions

To ensure the accuracy and feasibility of the iteration results, the condition that the difference between the maximum and minimum fitness values should not exceed 5% is combined with an additional condition: the discrete coefficient of the fitness values for all particles after each iteration must not exceed 5%. This adjustment helps optimize the final results of the iteration.

Finally, the updated particle velocity update formula is given in Equation (16).

$$v_{id}^{t+1} = \omega_d v_{id}^t + c_1^t r_1 (pBest_{id}^t(1 \pm r(0,1)) - x_{id}^t) + c_2^t r_2 (gBest_{id}^t(1 \pm r(0,1)) - x_{id}^t) \quad (16)$$

The flowchart for solving the multi-parameter optimization problem of damping isolation bearings using the improved APSO algorithm is shown in Figure 3.

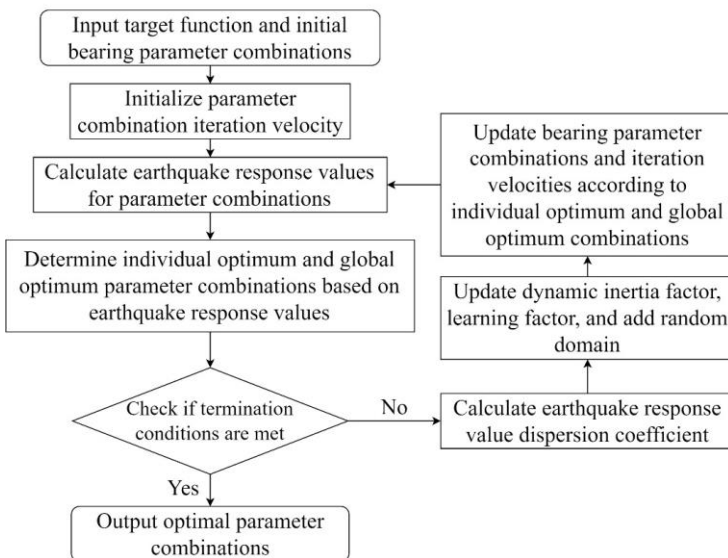


Figure 3. APSO algorithm for solving bearing optimal parameter combinations flowchart.

4 Engineering example

4.1 Finite element model and seismic input

4.1.1 Engineering Background

This study focuses on a four-span seismic isolation continuous girder bridge with a span of $4 \times 36\text{m}$. The superstructure of the bridge consists of a prestressed concrete box girder with a uniform cross-section, where the height of the girder is 1.8m , and the bridge deck width is 25.7m . The cross-section is of a single box with multiple chambers, and C50 concrete is used. The substructure consists of rectangular dual piers, each with a height of 9m and dimensions of $1.8\text{m} \times 2\text{m}$, constructed with C40 concrete. The pile foundation uses a group of piles, with a pile diameter of 1m and a height of 40m , made from C30 concrete. Each pier is equipped with one bearing, except for the two end abutments, which use Y4Q520 \times 135G0.8 type circular lead-core rubber bearings (LRB). The abutments are equipped with LNR(H)-d445 \times 136 type sliding horizontal force dispersing rubber bearings (LNR). To differentiate the piers at various locations, the bridge is numbered sequentially along the bridge direction as Pier 1#, Pier 2#, and Pier 3#. The longitudinal profile and plan layout of the bridge are shown in Figures 4 and 5.

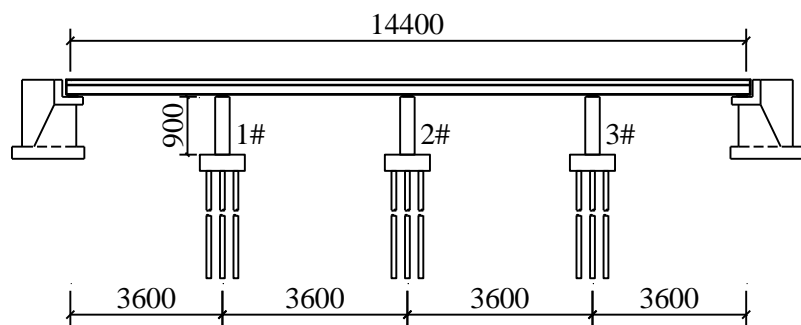


Figure 4. Bridge longitudinal section layout (unit: cm).

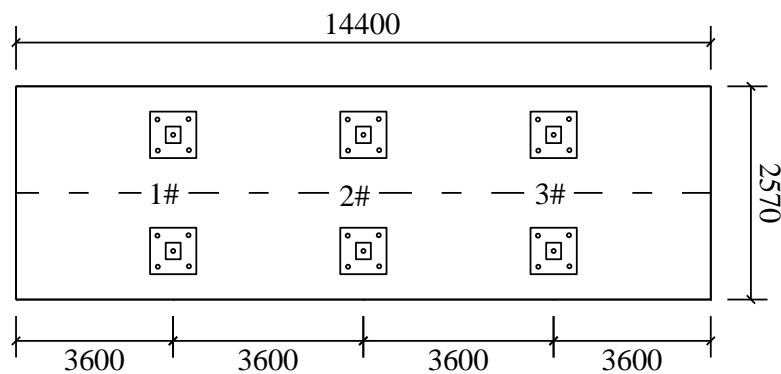


Figure 5. Bridge plan layout (unit: cm).

4.1.2 Support Bilinear Model

In the Midas software, the simulation of LRB bearings can directly use the linear characteristics of lead-core rubber bearings from the general connection characteristic values provided by the software. The simulation of the LNR bearings can be directly modeled using elastic connections. The equivalent linearization model represents the lead core rubber bearing as an approximate linear model, consisting of two linear mechanical parameters: equivalent stiffness and equivalent damping ratio. Such models are typically used for response spectrum analysis within the elastic range of structures²⁵. When subjected to external cyclic loading, the deformation of the lead core rubber bearing remains within the elastic-plastic range, and thus, the restoring force of the bearing is often modeled as bilinear²⁶. A common bilinear model for lead core rubber bearings is shown in Figure 6. The calculation formulas for the equivalent stiffness

and equivalent damping ratio are given in Equations (17) and (18), respectively.

$$K_{eff} = \frac{F_d}{D_d} = \frac{Q_d}{D_d} + K_2 \quad (17)$$

$$\xi_{eff} = \frac{2Q_d(D_d - \Delta_y)}{\pi D_d^2 K_{eff}} \quad (18)$$

where D_d represents the horizontal displacement of the seismic isolation bearing. According to the provisions of "Lead Core Seismic Isolation Rubber Bearings for Highway Bridges", the D_d value is taken as 50mm; Δ_y is the yield displacement of the seismic isolation bearing; Q_d is the characteristic strength of the seismic isolation bearing, defined as the value where the hysteresis curve intersects the shear force axis in the forward direction; K_{eff} denotes the equivalent stiffness of the seismic isolation bearing; K_1 is the pre-yield stiffness of the seismic isolation bearing; K_2 is the post-yield stiffness of the seismic isolation bearing; ξ_{eff} represents the equivalent damping ratio of the seismic isolation bearing.

As shown in Figure 6, the behavior of the lead core rubber bearing can be characterized by four parameters in the restoring force model: yield strength, equivalent stiffness, elastic stiffness, and yield stiffness. The restoring force in the bilinear model is calculated in two stages, with the formulas given in equations (19) and (20).

Pre-yield stage:

$$F_b = (K_1 - K_2)(D_d - \Delta_y) + K_2 D_d \quad (19)$$

Post-yield stage:

$$F_b = (K_1 - K_2)(D_d - \Delta_y) + K_2 D_d \quad (20)$$

where F_b represents the bearing's restoring force.

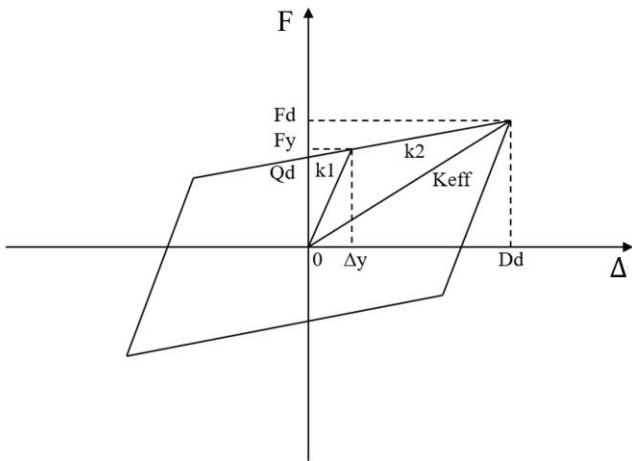
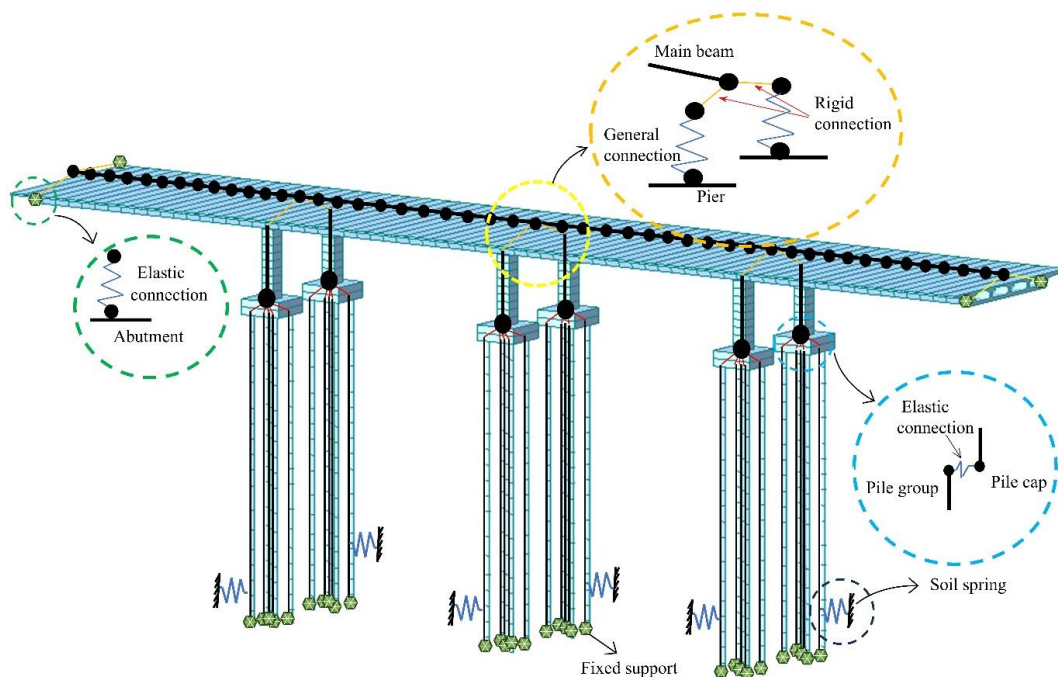


Figure 6. Finite element analysis model.

In the Midas simulation, when using the response spectrum method for bearing simulation analysis, the

356 software calls its linear characteristic values, including equivalent stiffness (K_{eff}) and vertical stiffness
 357 (K_v). Detailed parameter inputs for the bearing's linear characteristics can be referenced from the Midas
 358 Civil help file. The implementation of the bearing bilinear model and the finite element analysis model
 359 schematic in Midas are shown in Figure 7.
 360 In addition, it is important to acknowledge that the simulation accuracy of seismic isolation bearings
 361 significantly influences the reliability and precision of the structural analysis results. Figure 7 presents the
 362 finite element model of bearings, adopting a bilinear constitutive model in the Midas software. However,
 363 the simplifications inherent in these simulations—particularly the potential neglect of certain complex
 364 behaviors such as the "jumping-off" effect in friction pendulum bearings—could impact the predicted
 365 performance and optimization outcomes. Recent research has highlighted that neglecting this
 366 phenomenon may lead to deviations in evaluating bearing responses under seismic excitation. For instance,
 367 the study by Wei et al.²⁷, emphasizes that accurate modeling of the jumping-off effect significantly
 368 improves the precision of response predictions and contributes to more robust parameter optimization.
 369 Although the current approach provides acceptable accuracy within the linear and bilinear modeling
 370 assumptions, incorporating refined nonlinear behaviors could further validate the optimization results and
 371 extend the applicability of findings to practical engineering scenarios. Thus, while the current simulations
 372 in Figure 7 meet the immediate objectives, recognizing and addressing these complex bearing behaviors
 373 could substantially enhance the comprehensiveness and reliability of seismic isolation performance
 374 analyses.

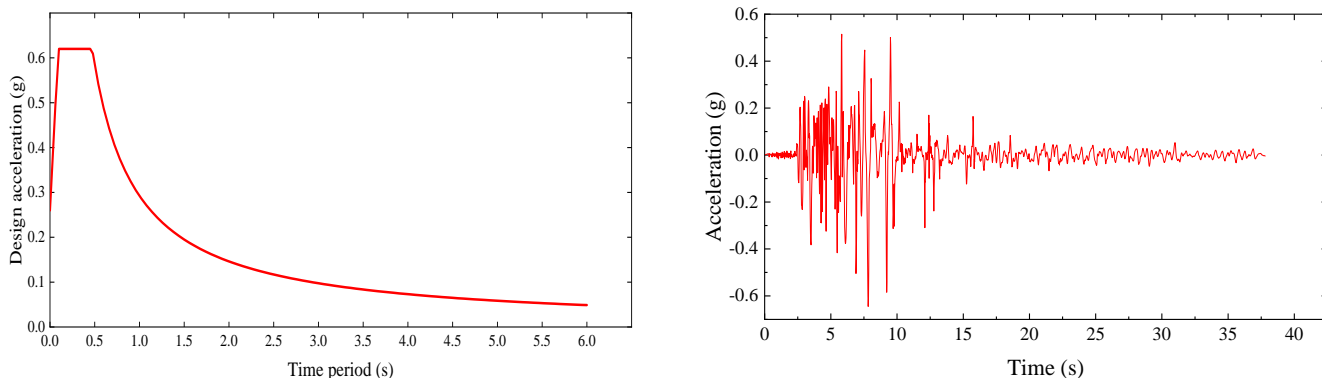


375
 376 **Figure 7.** Finite element analysis model.

377 **4.1.3 Earthquake input**

378 This study uses the "Seismic Design Code for Highway Bridges" (JTG/T2231-01-2020) to plot the design
 379 response spectrum, which serves as the target spectrum, as shown in Figure 8. The seismic isolation
 380 continuous beam bridge selected in this paper is located at a site with a basic earthquake intensity of 8
 381 degrees and a site category of Class III. According to the regulations, the vertical earthquake effect is not
 382 considered. According to the code, the acceleration time history should consist of no fewer than three sets.
 383 Therefore, three earthquake waves—James, Imperial Valley-01, and Parkfield—were selected from the

384 PEER strong-motion database. Among the earthquake responses caused by these three waves, the James
 385 earthquake wave induces the maximum seismic response in the bridge. Consequently, this study analyzes
 386 the parameter optimization of the pre-yield stiffness of the bearings under the effect of this seismic wave.
 387 The evaluation criteria for the optimization include the pier top displacement, pier bottom shear force,
 388 and their weighted sum. The time history of the acceleration at the pier top is shown in Figure 8.



389 (a) (b)

390 **Figure 8.** James’s earthquake wave. (a) target response spectrum. (b) earthquake time history excitation.

391 4.2 Single-parameter sensitivity-based optimization of seismic isolation bearing 392 parameters

393 To investigate the impact of various bearing parameters on the seismic performance of continuous girder
 394 bridges, this section uses a single-parameter sensitivity analysis under the James earthquake excitation.
 395 Specifically, one parameter (yield strength, pre-yield stiffness, or post-yield stiffness) is adjusted at a time
 396 while keeping the other parameters constant. The impact of these changes on the bridge's seismic
 397 performance is then evaluated. Although practical bridge design requires the evaluation of multiple
 398 earthquake waves, to visually demonstrate the impact of a single parameter on isolation effectiveness, this
 399 study selects the James earthquake wave as the focus of the analysis and optimizes each parameter
 400 individually.
 401

402 4.2.1 Design principles and parameter settings

403 Before analyzing the impact of individual parameters, some design principles and parameter ranges need
 404 to be established. The finite element model used in this section is the same as the one in Section 4.1, which
 405 includes the bridge’s geometric dimensions, material properties, and boundary conditions. The seismic
 406 input is based on the James earthquake record, adjusted according to relevant seismic design standards to
 407 represent a high-intensity seismic scenario²⁸.

408 In the nonlinear behavior of lead-core rubber bearings (LRB), three key parameters are crucial:

409 (1) Yield Strength (Q_y): This determines the energy dissipation capacity of the bearing, with a value
 410 range of 61 kN to 381.4 kN, with a step size of 35.6 kN.

411 (2) Pre-Yield Stiffness (K_1): This affects the elastic response of the bearing and the structural natural
 412 frequency, with a range of 4.5 kN/mm to 18.5 kN/mm, with a step size of 1.4 kN/mm.

413 (3) Post-Yield Stiffness (K_2): This reflects the bearing’s mechanical performance in the post-yield

stage, with a value range of 0.7 kN/mm to 2.95 kN/mm , with a step size of 0.25 kN/mm . For ease of comparison, this section extracts absolute values closely related to seismic performance (such as pier top displacement, bearing displacement, and pier bottom shear force) from the time history analysis results. These values are normalized when necessary to highlight the relative impact of parameter changes.

4.2.2 Bridge seismic response and bearing parameter optimization under different yield strengths

In this section's single-parameter sensitivity analysis, the yield strength Q_y is varied over ten different values while holding other bearing parameters constant. Time history analysis is performed using the James earthquake record. As shown in Figure 9, as Q_y increases, the pier top displacement decreases within a certain range. However, once the yield strength exceeds a certain threshold, it starts to increase again, indicating that moderate yield strength is beneficial for energy dissipation, while excessively high stiffness redirects more seismic force to the superstructure. Meanwhile, bearing displacement generally decreases as Q_y increases and remains within the allowable shear deformation range. This trend is also reflected in the distribution of pier bottom shear forces, where larger Q_y values reduce the force difference between the high pier (Pier #2) and the low pier (Pier #1), leading to a more balanced seismic force distribution across the bridge piers.

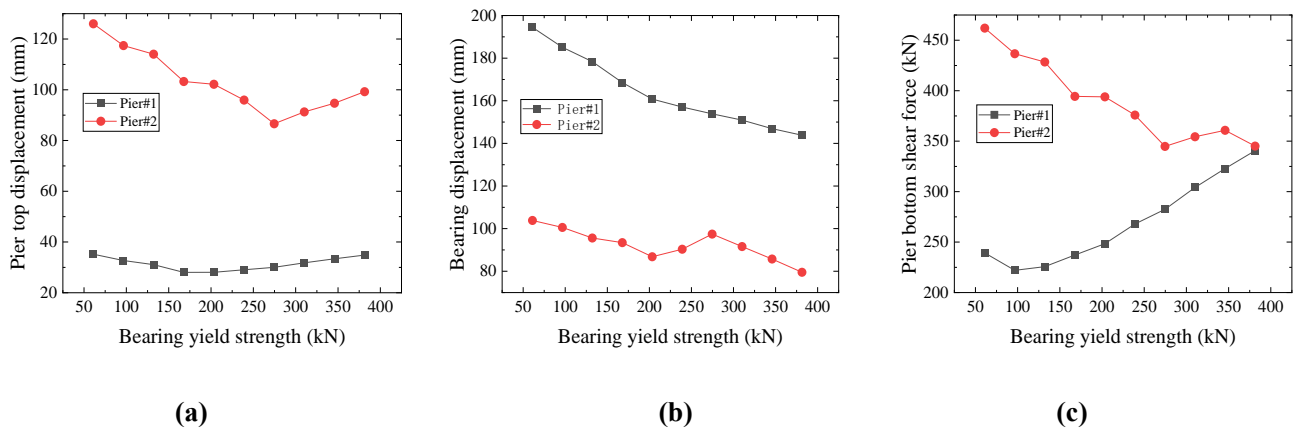


Figure 9. Bridge seismic response under different bearing yield strengths. (a) pier top displacement. (b) bearing displacement. (c) pier bottom shear force

Based on these results, this study minimizes the pier top displacement, minimizes the pier bottom shear force, and uses a weighted combination of both as objectives for the single-parameter optimization under the James earthquake. Table 1 lists the optimal values for each objective and the corresponding improvements relative to the original design of Y4Q520×135G0.8. When $Q_y \approx 274.6 \text{ kN}$, the pier top displacement decreases by approximately 21.17%, while $Q_y \approx 167.8 \text{ kN}$ results in an 18.27% reduction in pier bottom shear force. The weighted combination of displacement and shear force results in reductions of 14.36% and 18.27%, respectively. These results demonstrate that moderate yield strength achieves a balance between energy dissipation and pier bottom force, providing a more uniform force distribution and improved seismic performance for the continuous girder bridge under strong seismic excitation.

Table 1. Optimization effects on seismic response at optimal yield strengths.

Optimization	Optimal yield	Resulting	Resulting shear	Displacement	Shear force
--------------	---------------	-----------	-----------------	--------------	-------------

objective	strength (kN)	displacement (mm)	force (kN)	reduction (%)	reduction (%)
Minimize pier top displacement	274.6	293.26	-	21.17%	-
Minimize bearing displacement	167.8	-	1450.4	-	18.27%
Balanced shear-displacement	167.8	318.58	1450.4	14.36%	18.27%

Note: At this point, the bearing's pre-yield stiffness is 9.3 kN/mm, and post-yield stiffness is 1.4 kN/mm.

4.2.3 Bridge seismic response and bearing parameter optimization under pre-yield stiffness

When analyzing the pre-yield stiffness (K_1), ten different values for K_1 were set while holding other bearing parameters constant, and time history analysis was conducted using the James earthquake record. As shown in Figure 10, with increasing K_1 , the pier top displacement shows a linear decreasing trend, and bearing displacement slightly decreases, remaining within the allowable deformation range. This indicates that larger K_1 effectively enhances the initial stiffness of the bearing while avoiding excessive deformation. Regarding pier bottom shear force, Pier #1 is less affected by K_1 , while Pier #2 shows a significant reduction in shear force as K_1 increases. This suggests that for relatively taller piers, greater initial stiffness better resists lateral seismic forces.

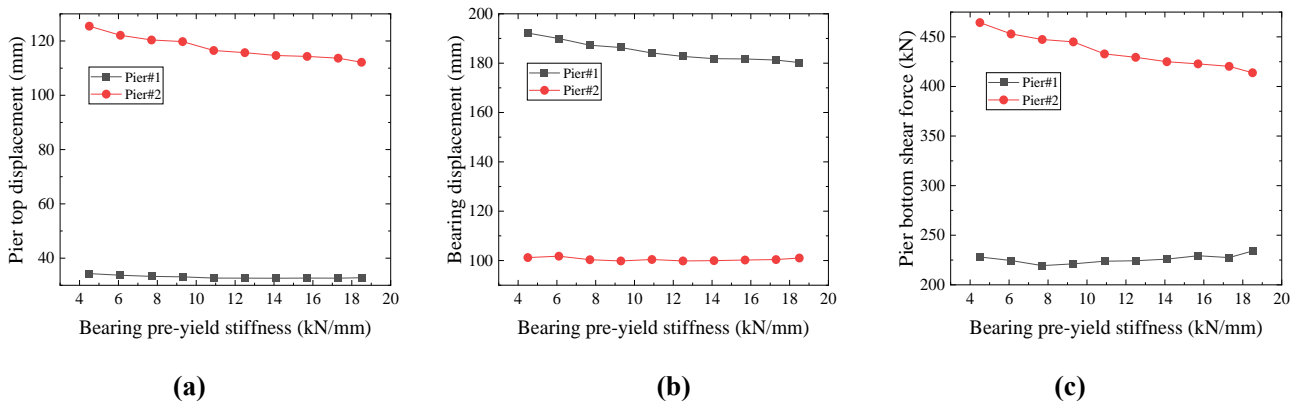


Figure 10. Bridge seismic response under different pre-yield stiffness of bearings. (a) pier top displacement. (b) bearing displacement. (c) pier bottom shear force

Since the James earthquake induces the strongest excitation among the selected waveforms, the single-parameter optimization aimed to minimize pier top displacement, minimize pier bottom shear force, and minimize the weighted combination of both. The final results are shown in Table 2. When $K_1 \approx 18.5 \text{ kN/mm}$, the pier top displacement decreases by about 4.46% compared to the original design of Y4Q520×135G0.8. $K_1 \approx 17.3 \text{ kN/mm}$ is more favorable for reducing pier bottom shear force (1.36%) and provides a balanced control over both displacement and force in the weighted objective. Although the improvements are not significant, they highlight the fine-tuning effect of pre-yield stiffness on the bridge's

464 initial seismic response and suggest that even small adjustments to K_1 may lead to a more reasonable
 465 seismic force distribution between tall and short piers.

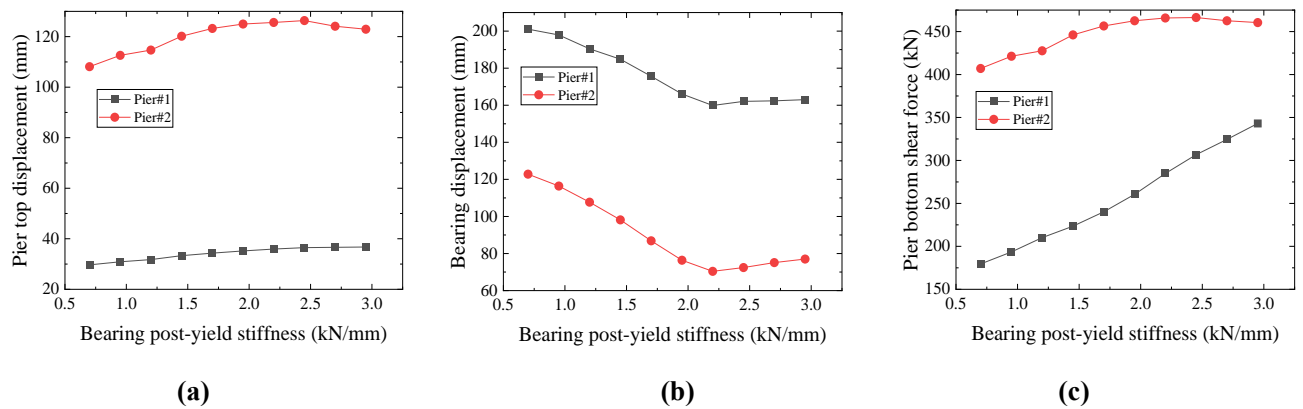
466 **Table 2.** Optimization effects on seismic response at pre-yield stiffness.

Optimization objective	Optimal yield strength (kN)	Resulting displacement (mm)	Resulting shear force (kN)	Displacement reduction (%)	Shear force reduction (%)
Minimize pier top displacement	18.5	355.4	-	4.46%	-
Minimize bearing displacement	17.3	-	1750.6	-	1.36%
Balanced shear-displacement	17.3	357.88	1750.6	3.8%	1.36%

467 **Note:** At this point, the bearing yield strengths is 96 kN/mm, and post-yield stiffness is 1.4 kN/mm.

468 4.2.4 Bridge seismic response and bearing parameter optimization under pre-yield stiffness

469 In this section, the impact of post-yield stiffness K_2 on the seismic performance of the continuous girder
 470 bridge under the James earthquake is examined. As shown in Figure 11, the pier top displacement
 471 increases almost linearly with K_2 , while bearing displacement initially decreases with increasing K_2 ,
 472 reaching a turning point near $K_2 \approx 2.2 \text{ kN/mm}$, and then increases again. At the same time, pier bottom
 473 shear force continues to increase with K_2 . Although these response curves do not show clear minima or
 474 maxima within the test range, bearing displacement remains below its ultimate shear capacity, indicating
 475 that stiffness variations within this range will not cause the bearings to exceed the safe deformation limits.



476
 477
 478 **Figure 11.** Bridge seismic response under different post-yield strengths of bearings. (a) pier top displacement. (b) bearing
 479 displacement. (c) pier bottom shear force

480 Table 3 shows that when $K_2 \approx 0.7 \text{ kN/mm}$, the displacement and shear force improve by approximately
 481 9.96% and 13.68%, respectively, compared to the original design of Y4Q520×135G0.8. Although these
 482 improvements are not substantial, they emphasize the critical role of post-yield stiffness in seismic force
 483 distribution. If K_2 is too high, it increases the displacement demand on the bridge piers, while

moderately lower K_2 is more advantageous in achieving a balanced control between deformation and reduced force.

Table 3. Optimization effects on seismic response at post-yield stiffness.

Optimization objective	Optimal yield strength (kN)	Resulting displacement (mm)	Resulting shear force (kN)	Displacement reduction (%)	Shear force reduction (%)
Minimize pier top displacement	0.7	334.96	-	9.96%	-
Minimize bearing displacement	0.7	-	1532	-	13.68%
Balanced shear-displacement	0.7	334.96	1532	9.96%	13.68%

Note: At this point, the bearing yield strengths is 96 kN/mm, and per-yield stiffness is 9.3 kN/mm.

4.3 Multi-parameter optimization of seismic isolation bearings based on orthogonal experiment

4.3.1 Principles of orthogonal experiment

The orthogonal experimental method provides a systematic framework for exploring the optimal combination of multiple parameters. In seismic isolation bearing design, three critical parameters—yield strength, pre-yield stiffness, and post-yield stiffness—often interact with one another. By selecting representative levels for the parameters and arranging them in an orthogonal table, it is possible to significantly reduce the number of simulations required while maintaining the robustness of the optimization results. The orthogonal experiment primarily revolves around the use of orthogonal tables, which combine different values of bearing parameters through orthogonal combinations. This ensures that each non-linear characteristic parameter appears evenly across all possible combinations, allowing each parameter to independently influence the optimization results and enabling the identification of the optimal parameter combination. Orthogonal tables are typically denoted as $L_n(b^c)$, where L represents the orthogonal table, n represents the total number of experiments, c represents the number of factors under consideration, and b represents the number of levels of each factor. Factors refer to the specific parameters that influence the experimental results—in this case, the non-linear characteristic parameters of the bearings; levels refer to the specific values of these factors—here, the specific values of the bearing's non-linear characteristics. In this study, range analysis is primarily used to evaluate the impact of each factor on the experimental results.

4.3.2 Parameter settings

The numerical model and the range of values for the bearing's non-linear characteristic parameters are the same as those in Section 4.2. The factors and their levels used in this orthogonal experiment are shown in Table 4.

Table 4. Orthogonal test factor levels.

Factors	Values at different levels		
	Level 1	Level 2	Level 3
Yield strength (kN)	140	220	300
Pre-yield stiffness (kN/mm)	8	11.5	15

Post-yield stiffness (kN/mm)	1.26	1.83	2.4
------------------------------	------	------	-----

Based on these values, a 3-factor, 3-level orthogonal table $L9(3^3)$ is employed for the experiment, with the specific orthogonal design shown in Table 5. According to the orthogonal table, only 9 simulations are required for the three-factor, three-level simulation experiments, significantly reducing the workload.

Table 5. Orthogonal table for bearing nonlinear characteristic parameters.

Test number	Factors		
	Yield strength (kN)	Pre-yield stiffness (kN/mm)	Post-yield stiffness (kN/mm)
1	140	8	1.26
2	140	11.5	2.4
3	140	15	1.83
4	220	8	2.4
5	220	11.5	1.83
6	220	15	1.26
7	300	8	1.83
8	300	11.5	1.26
9	300	15	2.4

4.3.3 Multi-parameter optimization of seismic isolation bearings for continuous girder bridges

For the seismic design optimization based on the seismic responses induced by three earthquake waves, the James earthquake wave, which induces the largest seismic response among the three, is selected for this section. The time history analysis method is used to optimize the bearing parameters, with the evaluation criteria being the pier top displacement, pier bottom shear force, and the weighted sum of both. The results of the orthogonal experiment analysis and calculations for the seismic isolation linear continuous girder bridge are shown in Table 6.

Table 6. The evaluation index and calculation result are analyzed by orthogonal experiment.

Test number	Evaluation indicators		
	Pier top displacement (mm)	Pier bottom shear force (kN)	Weighted sum of both
1	332.29	1699.3	0.73
2	364.81	2061.28	1.81
3	341.3	1814.1	1.06
4	356.74	2155.6	1.91
5	321.86	1934.58	1.09
6	272.7	1659.1	0
7	330.62	2075.72	1.47
8	298.16	1775.24	0.51
9	350.17	2128.74	1.79

Range analysis is performed for different evaluation criteria and calculation results. The analysis results are as follows:

(1) The range calculation results for the pier top displacement as the evaluation criterion are shown in Table 7.

Table 7. The results of range analysis with pier top displacement as the evaluation index.

	Level	Factor 1(yield strength)	Factor 2(pre-yield stiffness)	Factor 3(post-yield stiffness)
K_i	1	1038.39	1019.65	903.15
	2	951.3	984.82	993.77

value	3	978.94	964.16	1071.72
\bar{K}_i	1	346.13	339.88	301.05
	2	317.1	328.27	331.26
value	3	326.31	321.39	357.24
Optimal level		1	2	3
R value		135.01	29.03	18.5

The optimal parameter combinations for the bearings under the orthogonal experiment, based on the pier top displacement, and the optimization rate relative to the original engineering bearing Y4Q520×135G0.8 are shown in Table 8.

Table 8. Optimal parameter combinations and optimization rates for bearings.

Yield strength (kN)	Pre-yield stiffness (kN/mm)	Post-yield stiffness (kN/mm)	Resulting displacement (mm)	Optimization rate
220	15	1.26	272.7	26.69%

(2) The range calculation results for the pier bottom shear force as the evaluation criterion are shown in Table 9.

Table 9. Range analysis results for pier bottom shear force as the evaluation indicator.

	Level	Factor 1(yield strength)	Factor 2(pre-yield stiffness)	Factor 3(post-yield stiffness)
K_i	1	5574.68	5930.62	5133.64
	2	5749.28	5771.1	5824.4
value	3	5979.7	5601.94	6345.62
\bar{K}_i	1	1858.23	1976.87	1711.21
	2	1916.43	1923.7	1941.47
value	3	1993.23	1867.31	2115.21
Optimal level		1	3	1
R value		135.01	109.56	403.99

The optimal parameter combinations for the bearings under the orthogonal experiment, based on pier bottom shear force, and the optimization rate relative to the original engineering bearing Y4Q520×135G0.8 are shown in Table 10.

Table 10. The combination of the optimal parameters of the support and the optimization rate.

Yield strength (kN)	Pre-yield stiffness (kN/mm)	Post-yield stiffness (kN/mm)	Resulting displacement (mm)	Optimization rate
140	15	1.26	1594.64	10.15%

(3) The range calculation results for the weighted sum of shear force and displacement as the evaluation criterion are shown in Table 11.

Table 11. Results of parameter optimization with shear force-displacement weighted sum as the target function.

	Level	Factor 1(yield strength)	Factor 2(pre-yield stiffness)	Factor 3(post-yield stiffness)
K_i	1	3.6	4.11	1.24
	2	3	3.41	3.61
value	3	3.77	2.84	5.51
\bar{K}_i	1	1.2	1.37	0.41
	2	1	1.14	1.2
value	3	1.26	0.95	1.84
Optimal level		2	3	1
R value		0.25	0.42	1.42

The optimal parameter combinations for the bearings under the orthogonal experiment, based on the weighted sum of shear force and displacement, and the optimization rate relative to the original engineering bearing Y4Q520×135G0.8 are shown in Table 12.

Table 12. Optimal parameter combinations and optimization rates for bearings.

Yield strength (kN)	Pre-yield stiffness (kN/mm)	Post-yield stiffness (kN/mm)	Resulting displacement (mm)	Resulting shear force (kN)	Displacement reduction (%)	Shear force reduction (%)
220	15	1.26	272.7	1659.1	10.15%	6.52%

In summary, the seismic response of the seismic isolation linear girder bridge with the optimal parameter combinations obtained through the orthogonal experiment shows a significant reduction. Compared to the original engineering bearing Y4Q520×135G0.8, the pier top displacement decreases by 26.69% when using displacement as the evaluation criterion; the shear force decreases by 10.15% when using pier bottom shear force as the evaluation criterion; and the weighted sum of displacement and shear force shows a reduction of 10.15% in displacement and 6.52% in shear force. The optimization effect is clear. Compared to parameter optimization using single-parameter sensitivity analysis, the multi-parameter optimization of the bearing using the orthogonal experiment yields better results and significantly reduces the workload.

4.4 Multi-Parameter Optimization of Seismic Isolation Bearings Based on the APSO

Algorithm

4.4.1 Bearing multi-parameter optimization with pier bottom shear force as the objective function

To verify the effectiveness and applicability of the APSO algorithm for multi-parameter optimization of seismic isolation bearings, this section employs time-history analysis under the James earthquake excitation. The APSO algorithm is used to iteratively optimize 15 initial bearing parameter combinations for a linear seismic isolation continuous girder bridge, with the objective function defined as the pier bottom shear force. This iterative process creates an optimization space within which the optimal parameter combination is identified to refine the bearing parameters further. To visually represent the distribution of particles in the optimization space, the projections of particles along different parameter directions are illustrated as scatter plots (see Figure 12).

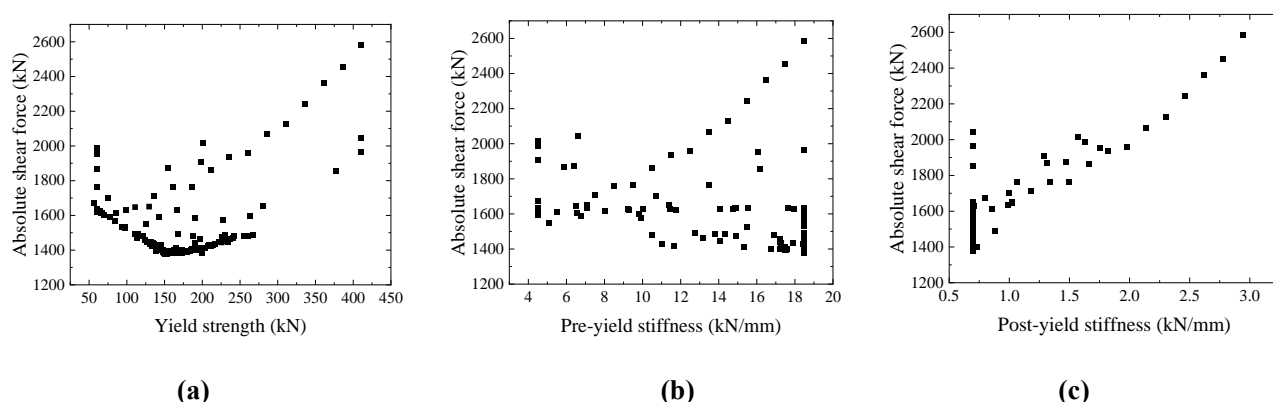
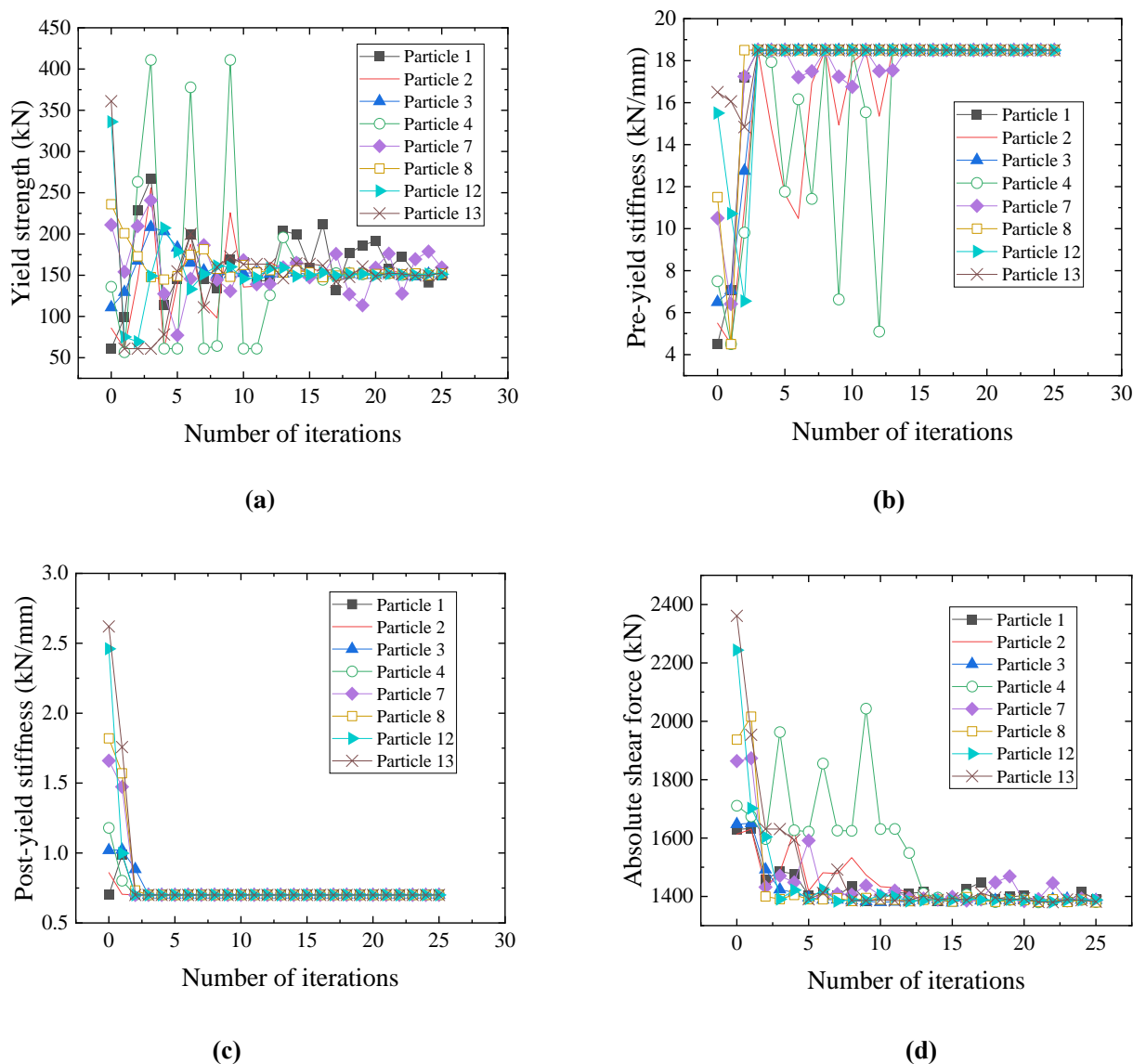


Figure 12. The distribution of iterative particles projected in different directions in shear optimization space. (a) yield strength direction. (b) pre-yield stiffness direction. (c) post-yield stiffness direction

It is observed that the projection in the yield strength direction forms a V-shape, with particles gradually concentrating around 150kN; the projection in the pre-yield stiffness direction converges toward the maximum value of 18.5kN / mm; and the projection in the post-yield stiffness direction converges toward

574 the minimum value of $0.7\text{kN}/\text{mm}$. This uniform distribution indicates that the particle swarm covers
 575 nearly the entire parameter range during optimization. To further demonstrate the iterative paths and
 576 results, the trajectories of selected particles (8 randomly chosen for clarity) are plotted as line graphs in
 577 Figure 13.



580
581
582 **Figure 13.** Iteration particle projections along parameter directions in the optimization space. (a) yield strength direction. (b) pre-
 583 yield stiffness direction. (c) post-yield stiffness direction. (d) objective function value direction

584 Based on the APSO algorithm, Table 13 presents the optimal bearing parameter combinations—using pier
 585 bottom shear force as the objective function—and their corresponding optimization rates relative to the
 586 original engineering bearing Y4Q520×135G0.8.

587 **Table 13.** The optimal parameter combination and optimization rate of the support.

Yield strength (kN)	Pre-yield stiffness (kN/mm)	Post-yield stiffness (kN/mm)	Resulting displacement (mm)	Optimization rate
150	18.5	0.7	1378.4	22.2%

588 From Figure 13 and Table 13, it is evident that:

- 589 (1) Except for the yield strength direction, where convergence is relatively slow (particles begin
 590 converging around the 20th iteration and essentially converge by the 25th), the pre-yield and post-yield
 591 stiffness directions achieve convergence more rapidly (approximately by the 15th and 4th iterations,

respectively). This difference indicates that convergence in the yield strength direction is the slowest and plays a decisive role in the final optimization outcome.

(2) The objective function stabilizes after roughly 20 iterations. Compared to the initial parameter combinations, the optimized parameters reduce the absolute value of the pier bottom shear force by 15% at minimum and up to 43% at maximum; relative to the original bearing Y4Q520×135G0.8, the reduction is about 22.2%, demonstrating a significant improvement.

4.4.2 Bearing multi-parameter optimization with pier top displacement as the objective function

Under the same James earthquake excitation and using time-history analysis, this section applies the APSO algorithm to iteratively optimize 15 initial bearing parameter combinations for the linear seismic isolation continuous girder bridge, with the objective function defined as the pier top displacement. An optimization space is thereby established for identifying the optimal parameter combination. To intuitively display the distribution of particles in the optimization space, scatter plots of particle projections along different parameter directions are provided (see Figure 14).

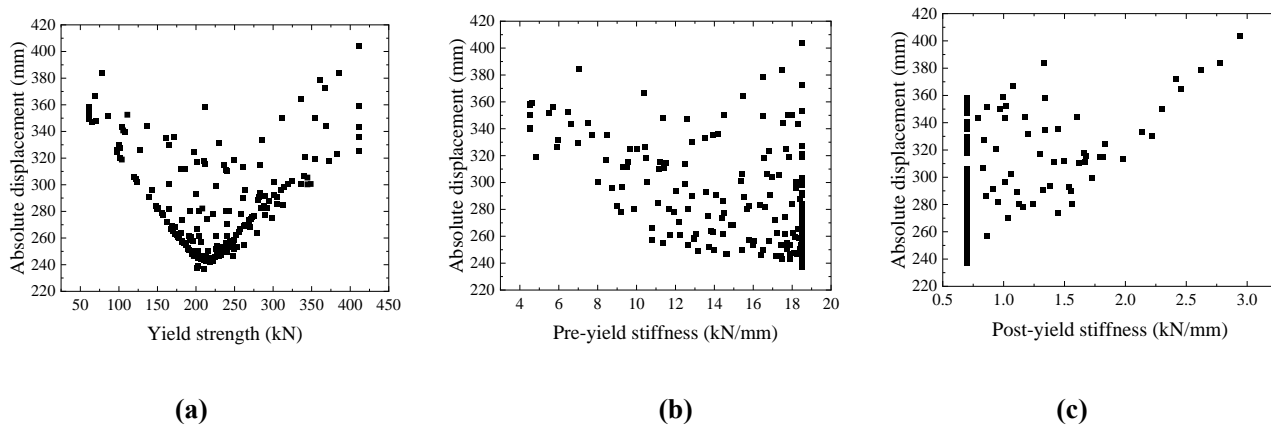


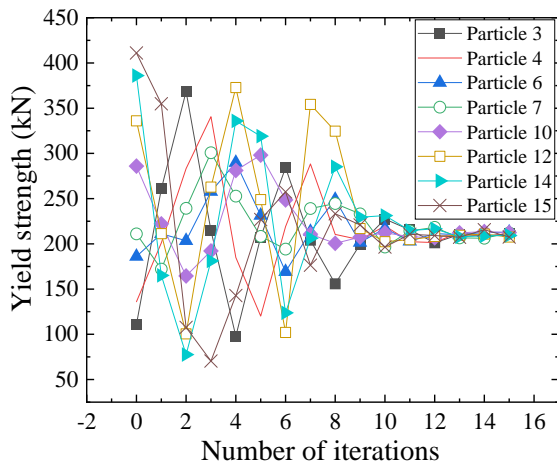
Figure 14. The distribution of iterative particles projected in different directions in displacement optimization space. (a) yield strength direction. (b) pre-yield stiffness direction. (c) post-yield stiffness direction

The results show that:

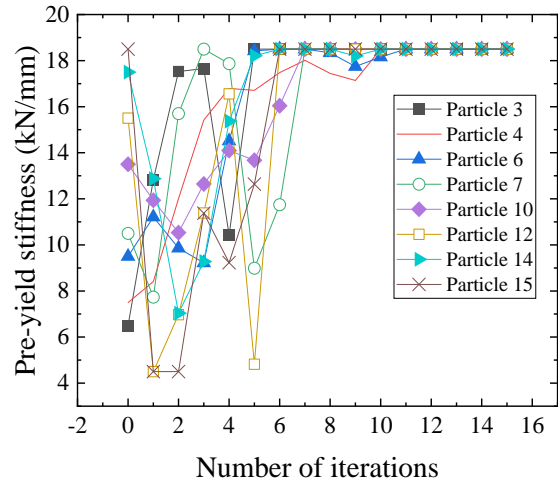
(1) The improved APSO algorithm enables particles to search a broader parameter space with a more uniform distribution, effectively avoiding local optima and accelerating the discovery of the global optimum.

(2) In the yield strength direction, the particle distribution exhibits a V-shape with convergence around $210kN$; in the pre-yield stiffness direction, particles concentrate at the maximum value of $18.5kN/mm$; and in the post-yield stiffness direction, they converge toward the minimum value of $0.7kN/mm$.

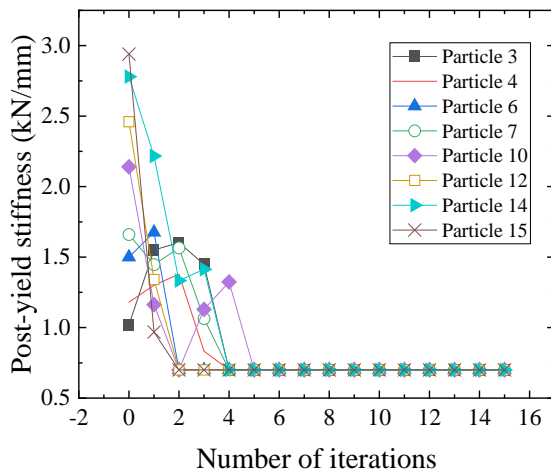
For clarity, the iterative trajectories of 8 randomly selected particles are depicted in Figure 15.



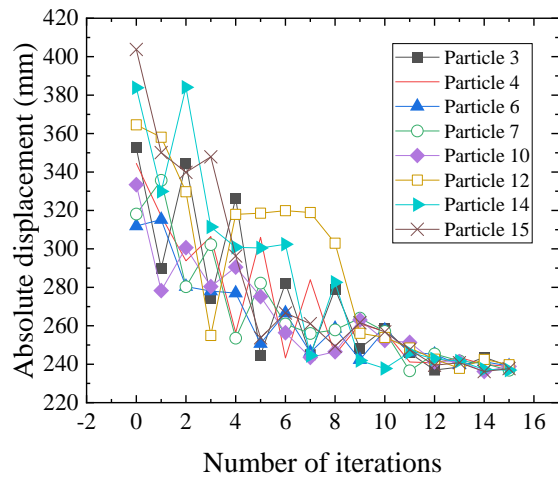
(a)



(b)



(c)



(d)

Figure 15. Iteration particle projections along parameter directions in the optimization space. (a) yield strength direction. (b) pre-yield stiffness direction. (c) post-yield stiffness direction. (d) objective function value direction

Table 14 presents the optimal parameter combinations obtained with pier top displacement as the objective function, along with the corresponding optimization rates relative to the original bearing Y4Q520×135G0.8.

Table 14. The optimal parameter combination and optimization rate of the support.

Yield strength (kN)	Pre-yield stiffness (kN/mm)	Post-yield stiffness (kN/mm)	Resulting displacement (mm)	Optimization rate
210	18.5	0.7	236.96	36.6%

Analysis of Figure 15 and Table 14 reveals that:

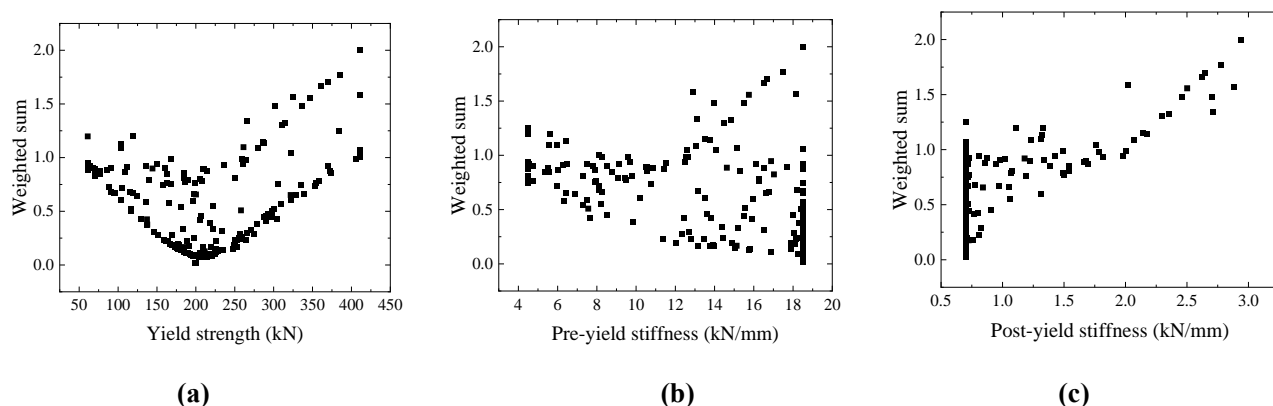
(1) Although convergence in the yield strength direction remains slower, starting around the 10th iteration and essentially converging by the 15th iteration, the pre-yield stiffness and post-yield stiffness directions converge by approximately the 10th and 5th iterations, respectively. Overall, the total number of iterations is greatly reduced, resulting in an approximate 40% increase in convergence speed.

(2) The objective function stabilizes after about 11 iterations, with an overall convergence speed improvement of approximately 45%. Compared to the initial parameter combinations, the optimized parameters reduce the absolute pier top displacement by 23.8% at minimum and 41.2% at maximum;

635 relative to the original bearing Y4Q520×135G0.8, the displacement is reduced by 36.6%, confirming a
 636 significant optimization effect.

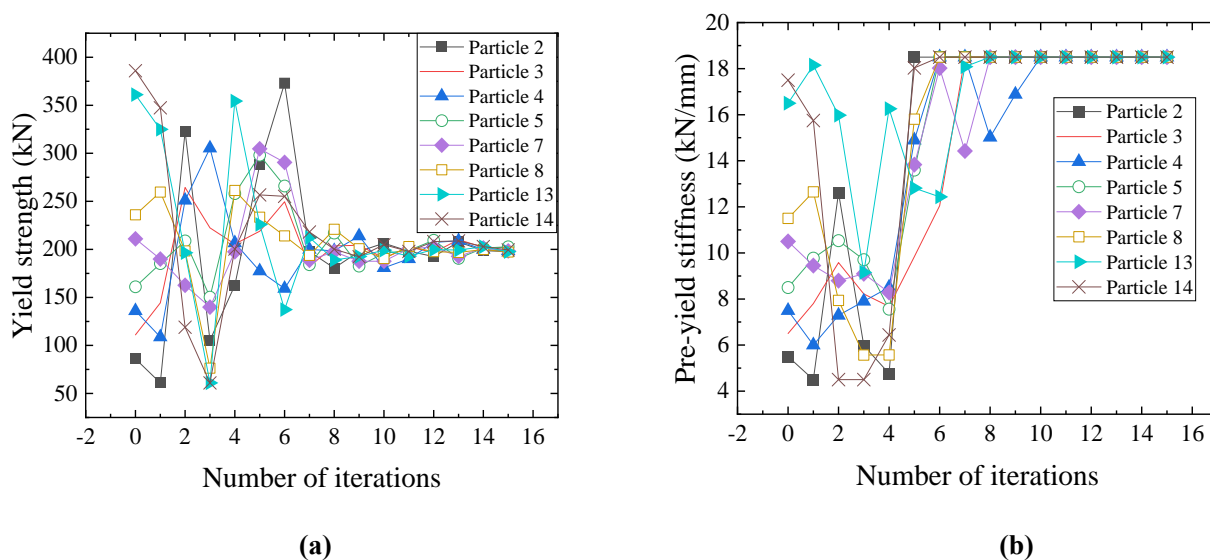
637 **4.4.3 Bearing multi-parameter optimization with a weighted sum of shear force and displacement**
 638 **as the objective function**

639 In practical seismic design, multiple seismic responses are sometimes considered simultaneously.
 640 Therefore, under the James earthquake excitation and using time-history analysis, the improved APSO
 641 algorithm is employed with the objective function defined as the weighted sum of pier bottom shear force
 642 and pier top displacement to optimize the bearing parameters.

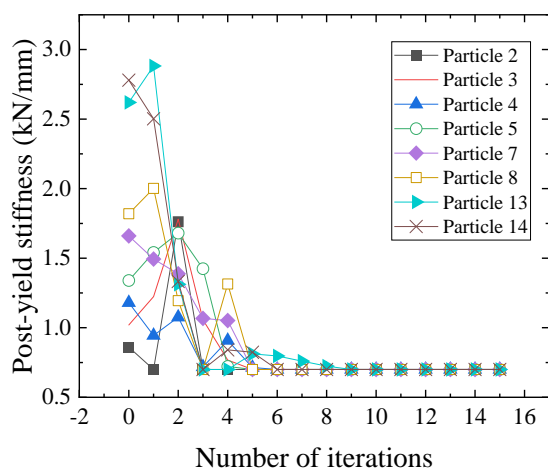


643
 644
 645 **Figure 16.** Distribution of iteration particle projections in shear force-displacement weighted optimization space. (a) yield strength
 646 direction. (b) pre-yield stiffness direction. (c) post-yield stiffness direction

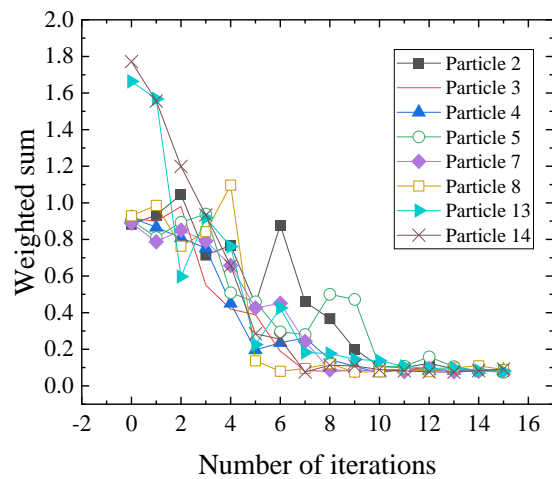
647 To visually display the distribution of particle parameter combinations within the optimization space,
 648 scatter plots of particle projections along various parameter directions are provided (see Figure 16). It is
 649 observed that the yield strength direction exhibits a V-shaped distribution with convergence around
 650 199.7kN ; the pre-yield stiffness direction converges at the maximum value of 18.5kN / mm ; and the post-
 651 yield stiffness direction converges at the minimum value of 0.7kN / mm . To further illustrate the iterative
 652 paths and outcomes, the trajectories of 8 randomly selected particles are plotted as line graphs in Figure
 653 17.



654
 655



(c)



(d)

Figure 17. Iteration particle projections along parameter directions in the optimization space. (a) yield strength direction. (b) pre-yield stiffness direction. (c) post-yield stiffness direction. (d) objective function value direction

Table 15 shows the optimal parameter combinations achieved using the weighted sum objective function, along with their corresponding optimization rates relative to the original bearing Y4Q520×135G0.8.

Table 15. The optimal parameter combination and optimization rate of the support.

Yield strength (kN)	Pre-yield stiffness (kN/mm)	Post-yield stiffness (kN/mm)	Resulting displacement (mm)	Resulting shear force (kN)	Displacement reduction (%)	Shear force reduction (%)
199.7	18.5	0.7	239.73	1383.26	35.8%	20.7%

From Figure 17 and Table 15, it can be concluded that:

(1) In the yield strength direction, convergence begins around the 9th iteration and is essentially complete by the 15th iteration; in the pre-yield stiffness direction, convergence is reached around the 10th iteration; and in the post-yield stiffness direction, convergence is achieved around the 8th iteration.

(2) The objective function stabilizes after approximately 10 iterations, with an estimated 50% improvement in convergence speed. When considering both shear force and displacement simultaneously, the optimized parameters reduce the weighted sum objective function value—shear force is reduced by 14.3% at minimum and 43.6% at maximum, and displacement is reduced by 23.8% at minimum and 37.6% at maximum. Relative to the original bearing Y4Q520×135G0.8, shear force decreases by 20.7% and displacement by 35.8%, demonstrating a clear and effective optimization.

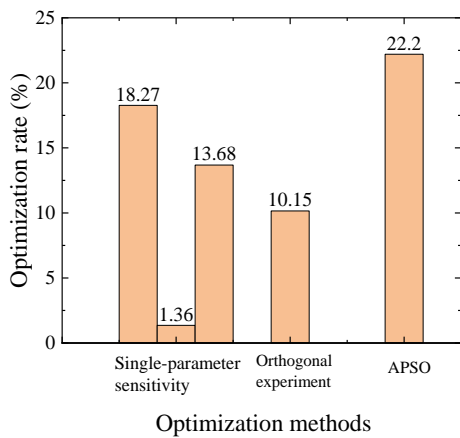
4.4 Optimization results analysis

Under the excitation of the James earthquake, the nonlinear characteristic parameters of the seismic isolation bearings for the isolation linear continuous girder bridge were optimized using different methods. The optimization results are presented in Table 16 and Figures 18–20.

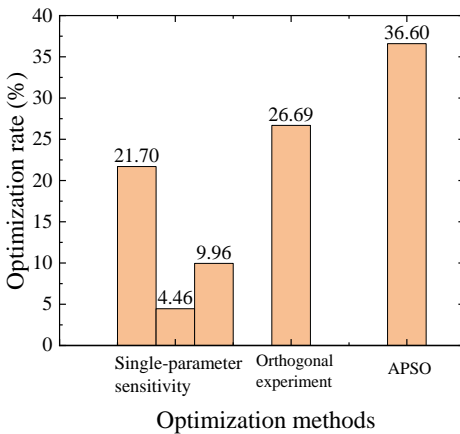
Table 16. Optimal bearing parameter combinations and optimization rates under different optimization methods.

Optimization methods	Target function	Parameter combinations				
		Yield strength (kN)	Pre-yield stiffness (kN/mm)	Post-yield stiffness (kN/mm)	Displacement optimization rate	Shear force optimization rate

		167.8	9.3	1.4	-	18.27%
	pier bottom					
	shear force	96	17.3	1.4	-	1.36%
		96	9.3	0.7	-	13.68%
Single-parameter sensitivity		274.6	9.3	1.4	21.17%	-
	pier top					
	displacement	96	18.5	1.4	4.46%	-
		96	9.3	0.7	9.96%	-
	shear force-	167.8	9.3	1.4	14.36%	18.27%
	displacement	96	17.3	1.4	3.80%	1.36%
		96	9.6	0.7	9.96%	13.68%
Orthogonal experiment	pier bottom					
	shear force	140	15	1.26	-	10.15%
	pier top					
	displacement	220	15	1.26	26.69%	-
	shear force-	220	15	1.26	10.15%	6.52%
	displacement					
	pier bottom					
	shear force	150	18.5	0.7	-	22.20%
APSO	pier top					
	displacement	210	18.5	0.7	36.60%	-
	shear force-					
	displacement	199.7	18.5	0.7	35.80%	20.70%



679 **Figure 18.** Results of parameter optimization with pier bottom shear force as the target function.



681 **Figure 19.** Results of parameter optimization with pier top displacement as the target function.

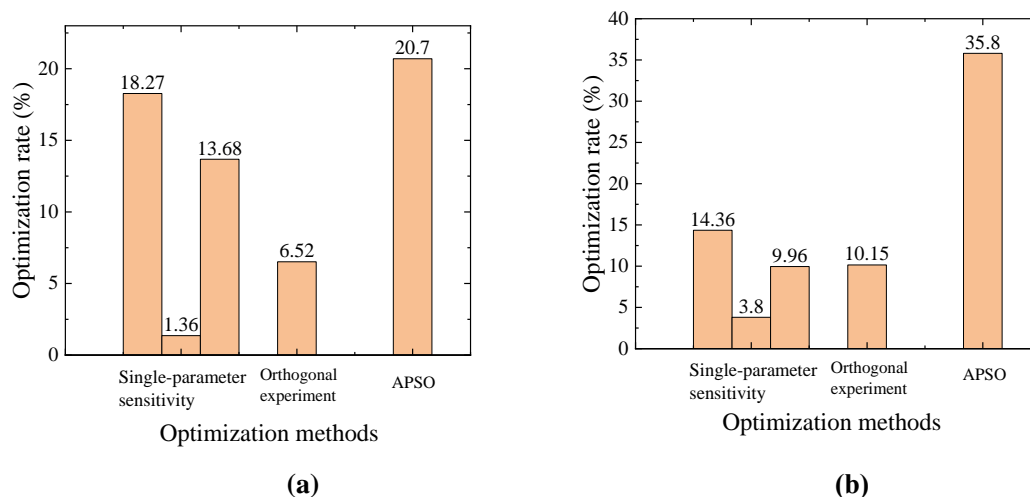


Figure 20. Results of parameter optimization with shear force-displacement weighted sum as the target function. (a) pier bottom shear force. (b) pier top displacement

From these results, it can be seen that although the computational burden of the APSO algorithm is greater than that of the orthogonal experiment, the improvement ultimately achieved by the APSO algorithm far exceeds the improvements achieved by the other two optimization methods. In the parametric optimization design for the bridge, the parameter combination derived from the single-parameter sensitivity analysis is highly dependent on the sensitivity of each parameter, which leads to significant variability in the optimization outcomes; although the orthogonal experiment approach requires relatively low effort, its optimization performance is comparatively insufficient. In contrast, the APSO algorithm provides an accurate and optimal parameter combination with the best optimization effect, albeit at the expense of a relatively higher computational workload.

5. Conclusion

This study presents an improved PSO algorithm, termed Adaptive Particle Swarm Optimization (APSO), specifically tailored for the multi-parameter optimization of seismic isolation bearings in continuous girder bridges. By adaptively adjusting inertia and learning factors, as well as refining the search strategy, APSO significantly enhances exploration of the design space. Numerical experiments demonstrate that APSO achieves three clear advancements:

1. APSO reduces the required computational iterations by approximately 40% compared to the standard PSO algorithm, thus markedly shortening optimization time while maintaining or even improving solution accuracy.
2. APSO efficiently handles complex interactions among multiple nonlinear characteristic parameters—including yield strength, pre-yield stiffness, and post-yield stiffness—making it particularly effective for both straight and curved continuous girder bridges. This efficiency ensures reliable convergence to the global optimum even in large-scale optimization scenarios.
3. APSO demonstrates robust scalability and adaptability, providing a practical solution for overcoming computational challenges associated with extensive search domains and intricate parameter dependencies in real-world structural engineering applications.

Despite these advancements, the current study has certain limitations. The proposed APSO algorithm's performance validation relies primarily on numerical simulations; experimental validations with physical models or real-world structures have not yet been conducted. Additionally, the algorithm's performance may vary under significantly different bridge configurations that were not explicitly

717 considered in this study.

718 Looking ahead, extending APSO to more sophisticated bearing configurations or diverse structural
719 components constitutes a valuable avenue for future research. Furthermore, integrating APSO with
720 advanced modeling frameworks and real-time monitoring technologies may facilitate dynamic adaptive
721 optimization, significantly enhancing seismic resilience and efficiency in bridge design across varying
722 loading conditions.
723

724 References:

- 725 1. Elnashai, A. S. & Di Sarno, L., *Fundamentals of earthquake engineering: from source to fragility*. (John Wiley & Sons,
726 2015).
- 727 2. Xie, H. *et al.*, Preliminary research and scheme design of deep underground in situ geo-information detection experiment
728 for Geology in Time. *INT J MIN SCI TECHNO* **34** 1 (2024).
- 729 3. Castillo, E., Mínguez, R. & Castillo, C., Sensitivity analysis in optimization and reliability problems. *RELIAB ENG SYST*
730 *SAFE* **93** 1788 (2008).
- 731 4. Amiri, G. G., Namiranian, P. & Amiri, M. S., Seismic response of triple friction pendulum bearing under near-fault ground
732 motions. *INT J STRUCT STAB DY* **16** 1550021 (2016).
- 733 5. Peng, Y., Ma, Y., Huang, T. & De Domenico, D., Reliability-based design optimization of adaptive sliding base isolation
734 system for improving seismic performance of structures. *RELIAB ENG SYST SAFE* **205** 107167 (2021).
- 735 6. Zhong, J., Wan, H., Yuan, W., He, M. & Ren, W., Risk-informed sensitivity analysis and optimization of seismic mitigation
736 strategy using Gaussian process surrogate model. *SOIL DYN EARTHQ ENG* **138** 106284 (2020).
- 737 7. Gur, S., Mishra, S. K. & Chakraborty, S., Stochastic optimization of shape-memory-alloy rubber bearing (SMARB) for
738 isolating buildings against random earthquake. *Structural Control and Health Monitoring* **21** 1222 (2014).
- 739 8. Pang, Y., He, W. & Zhong, J., Risk-based design and optimization of shape memory alloy restrained sliding bearings for
740 highway bridges under near-fault ground motions. *ENG STRUCT* **241** 112421 (2021).
- 741 9. Xia, Z. *et al.*, Model updating of an existing bridge with high-dimensional variables using modified particle swarm
742 optimization and ambient excitation data. *MEASUREMENT* **159** 107754 (2020).
- 743 10. Tran-Ngoc, H. *et al.*, An efficient approach to model updating for a multispan railway bridge using orthogonal
744 diagonalization combined with improved particle swarm optimization. *J SOUND VIB* **476** 115315 (2020).
- 745 11. Chen, Z., Cao, H., Ye, K., Zhu, H. & Li, S., Improved particle swarm optimization-based form-finding method for
746 suspension bridge installation analysis. *J COMPUT CIVIL ENG* **29** 4014047 (2015).
- 747 12. Li, J. *et al.*, Optimal sensor placement for long-span cable-stayed bridge using a novel particle swarm optimization algorithm.
748 *J CIV STRUCT HEALTH* **5** 677 (2015).
- 749 13. Quaranta, G., Marano, G. C., Greco, R. & Monti, G., Parametric identification of seismic isolators using differential
750 evolution and particle swarm optimization. *APPL SOFT COMPUT* **22** 458 (2014).
- 751 14. Zhang, J. *et al.*, AVA simultaneous inversion of prestack seismic data using particle swarm optimization. *J EARTH SCI-*
752 *CHINA* **29** 1390 (2018).
- 753 15. Wei, B. *et al.*, Seismic response prediction and fragility assessment of high-speed railway bridges using machine learning
754 technology. *STRUCTURES* **66** 106845 (2024).
- 755 16. Wei, B., Tan, H., Wan, K., Sun, Z. & Li, S., Seismic performance of railway bridges with novel ductile piers under near-
756 fault earthquakes. *TRANSP GEOTECH* **46** 101241 (2024).
- 757 17. Işık, M. F. *et al.*, A hybrid artificial neural network—Particle swarm optimization algorithm model for the determination of
758 target displacements in mid-rise regular reinforced-concrete buildings. *SUSTAINABILITY-BASEL* **15** 9715 (2023).
- 759 18. Wang, Z., Multi-objective Comprehensive Optimal Management of Construction Projects Based on Particle Algorithm.
760 *INFORMATICA-LITHUAN* **43** (2019).
- 761 19. Afzal, S., Shokri, A., Ziapour, B. M., Shakibi, H. & Sobhani, B., Building energy consumption prediction and optimization

- 762 using different neural network-assisted models; comparison of different networks and optimization algorithms. *ENG APPL*
763 *ARTIF INTEL* **127** 107356 (2024).
- 764 20. Fang, R. & Popole, Z., Multi-objective optimized scheduling model for hydropower reservoir based on improved particle
765 swarm optimization algorithm. *ENVIRON SCI POLLUT R* **27** 12842 (2020).
- 766 21. Lin, Y., Song, Z., Lv, R., Ma, A. & Dong, C., presented at the 2022 34th Chinese Control and Decision Conference (CCDC),
767 2022 (unpublished).
- 768 22. Wei, W. & Yi, Z., presented at the 2019 Chinese Control And Decision Conference (CCDC), 2019 (unpublished).
- 769 23. Wolpert, D. H. & Macready, W. G., No free lunch theorems for optimization. *IEEE T EVOLUT COMPUT* **1** 67 (1997).
- 770 24. Shi, Y. & Eberhart, R., presented at the 1998 IEEE international conference on evolutionary computation proceedings. IEEE
771 world congress on computational intelligence (Cat. No. 98TH8360), 1998 (unpublished).
- 772 25. Ozdemir, G. & Dicleli, M., Effect of lead core heating on the seismic performance of bridges isolated with LRB in near-
773 fault zones. *EARTHQ ENG STRUCT D* **41** 1989 (2012).
- 774 26. Mahamied, A., Yasin, A. A., Alzubi, Y., Al Adwan, J. & Mahamied, I., Influence of Vertical Irregularity on the Seismic
775 Behavior of Base Isolated RC Structures with Lead Rubber Bearings under Pulse-Like Earthquakes. *Health Monit* **17** 501
776 (2023).
- 777 27. Wei, B. *et al.*, Decoupled calculation and case study analysis of friction pendulum bearing considering the jumping-off
778 effect. *INT J STRUCT STAB DY* 2550195 (2024).
- 779 28. MoTotPsRo, C., Lead rubber bearing isolator for highway bridge. (2011).

780 **Author contributions**

781 Conceptualization, W.Z.; methodology, W.Z.; software, Y.Q.; validation, Y.Q., and Y.B.; data curation,
782 W.Z.; writing—original draft preparation, Y.B.; writing—review and editing, J.S., and T.K.; supervision,
783 W.Z.; project administration, J.S.; funding acquisition, W.Z. All authors have read and agreed to the
784 published version of the manuscript.

785 **Funding**

786 This research was funded by the Sichuan Natural Science Foundation of China under grant number
787 2024NSFSC0171.

788 **Competing interests**

789 The authors declare no competing interests.

790 **Data availability**

791 The data that support the findings of this study are available from the corresponding author upon
792 reasonable request.